Chemical Science

ROYAL SOCIETY OF CHEMISTRY

EDGE ARTICLE

View Article Online
View Journal | View Issue

Cite this: *Chem. Sci.*, 2023, **14**, 2735

All publication charges for this article have been paid for by the Royal Society of Chemistry

Structurally well-defined conjugated *meso*-aminoporphyrin oligomers analogous to polyanilines†

Ken-ichi Yamashita, *[abc] Shouichi Takeuchi[a] and Ken-ichi Sugiura *[a]

Polyaniline, which is formed by the oxidative polymerization of aniline, is a widely explored conducting polymer with several stable oxidation states, and can be applied in advanced materials, including sensing devices and electrochemical catalysts. The marriage of polyanilines with the diverse chemistry of porphyrins is expected to confer new properties, including a combination of electrical, optical, magnetic and chemical properties. Herein, we demonstrate that *meso*-aminodiarylporphyrin, a porphyrin analogue of aniline, undergoes oxidative oligomerization in an acidic solution under an oxygen atmosphere to yield stable oligomeric products that are analogous to fully oxidized polyanilines. The so-formed oligomers are composed of the same number of electron-rich porphyrinoid and electron-deficient quinoid moieties, and they exhibit a broad electronic absorption band in the near infrared (NIR) region, which is attributable to intramolecular charge transfer (ICT) transition from electron-rich porphyrinoid moieties to electron-deficient quinoid ones. The quinoid moieties in the oligomers could be reversibly reduced using sodium ascorbate to obtain all-porphyrinoid oligomers that resemble fully reduced polyanilines. The fully reduced oligomers do not exhibit the NIR ICT band. Furthermore, three types of partially reduced tetramers consisting of a single quinoid moiety were also obtained, among which two interconverted in solution. Their interconversion was significantly accelerated in the presence of a protic solvent. This result is consistent with the high electron conductivity of partially oxidized polyanilines following their protonation.

Received 21st November 2022
Accepted 16th February 2023

DOI: 10.1039/d2sc06387e

rsc.li/chemical-science

Introduction

π-Conjugated conductive polymers have been intensively studied over several decades.[1–3] One of the fundamental strategies for preparing them is to polymerize a π-conjugated monomer with an aromatic moiety (*e.g.*, benzene, thiophene, and pyrrole). Polyanilines (PANIs) are among the most popular conducting polymers, and their structure and redox behaviour have been studied extensively.[4–12] PANIs are synthesized by the chemical or electrochemical oxidation of aniline, and they have three stable redox states (Scheme 1): a fully reduced state (leucoemeraldine), a fully oxidized state (pernigraniline), and a partially oxidized state (emeraldine). In addition, protonated states of PANIs in all these redox states can be obtained by the protonation of the bridged nitrogen atoms. The electrochemical and spectroscopic properties of PANIs in these different states differ significantly. For example, leucoemeraldines are colourless, while emeraldines and pernigranilines are strongly coloured owing to intramolecular charge transfer (ICT) from benzenoid to quinoid moieties in their structures. Moreover, protonated emeraldines are known to have the highest conductivity. As their characteristic states are readily interconvertible under external stimuli, PANIs can be applied in

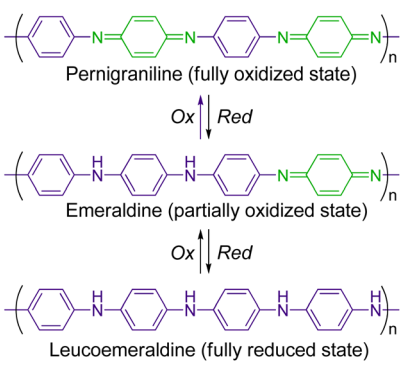

Scheme 1 Structure and redox behaviour of polyanilines (PANIs).

[a]*Department of Chemistry, Graduate School of Science and Engineering, Tokyo Metropolitan University, 1-1 Minami-Osawa, Hachioji, Tokyo 192-0397, Japan. E-mail: sugiura@porphyrin.jp*

[b]*Department of Chemistry, Graduate School of Science, Osaka University, 1-1 Machikaneyama, Toyonaka, Osaka, 560-0043, Japan. E-mail: yamashita-k@chem.sci.osaka-u.ac.jp*

[c]*Innovative Catalysis Science Division, Institute for Open and Transdisciplinary Research Initiatives (ICS-OTRI), Osaka University, Suita, Osaka 565-0871, Japan*

† Electronic supplementary information (ESI) available. See DOI: https://doi.org/10.1039/d2sc06387e

advanced materials, including sensing devices and electrochemical catalysts.[13–16]

For understanding the structure–property relationship of PANIs and/or their precise chemical modification, structurally well-defined monodisperse oligoanilines with various end functional groups have also been developed.[10,17–22] The replacement of the benzene ring with larger moieties affects their properties. Accordingly, analogous polymers of oligophenylenes, naphthalene, anthracene, and pyrene have been explored.[23–29]

Porphyrins are representative expanded aromatic molecules with an 18π aromatic character. Recently, π-conjugated linear porphyrin arrays (oligomers) have attracted considerable attention because of their unique properties.[30,31] Owing to their highly π-conjugated structure, oligomeric porphyrins exhibit narrow HOMO–LUMO gaps and exhibit characteristic optical properties, such as intense visible (vis)-near infrared (NIR) electronic absorption and nonlinear optical properties. Butadiyne-linked porphyrin oligomers[32,33] and triply-fused porphyrin oligomers[34,35] are representative examples of such porphyrins.

The marriage of PANIs to the chemistry of porphyrins and their metal complexes, represented by their strong light absorption and emission, redox, catalytic and magnetic properties, promises the development of new hybrid properties of conductive polymers. In 1987, two research groups reported the electrochemical oxidation of *meso*-tetrakis(aminophenyl) porphyrins to obtain electroactive polymer films; however, their chemical structures were not well defined.[36,37] Harvey *et al.* reported conjugated copolymers containing *meso*-diethynylporphyrin moieties[38] and Gust *et al.* conducted the electrochemical polymerization of *meso*-(4-aminophenyl)diarylporphyrins to obtain PANI-like linear porphyrin polymers.[39,40] However, the nearly orthogonal orientation between the porphyrin moieties and phenylene linkers disrupted effective π-conjugation; therefore, only fully reduced forms were obtained.

Replacing all benzene rings in PANI with porphyrin rings would be the simplest strategy for obtaining conjugated porphyrin polymers (oligomers) analogous to PANI. For this, *meso*-aminoporphyrins, porphyrin analogues of anilines, are promising monomer candidates. To the best of our knowledge, the oxidative polymerization/oligomerization of *meso*-aminoporphyrins has not been reported to date. On the other hand, Arnold *et al.* reported the copper-catalysed oxidative dimerization of Ni or Zn complexes of *meso*-aminotriarylporphyrins to obtain azo-linked dimers.[41–43] In addition, nitrogen-bridged porphyrin dimers have also been synthesized by palladium-catalysed coupling reactions.[44–47]

Recently, we investigated the synthesis and properties of *meso*-heteroatom-substituted porphyrins[48–50] and nonaromatic quinoidal porphyrins,[49,51–53] and reported the facile synthesis of free-base *meso*-aminoporphyrins.[50] Herein, we demonstrate that free-base *meso*-aminoporphyrin **1** undergoes aerobic oxidation under ambient acidic conditions to afford structurally well-defined π-conjugated *meso*-aminoporphyrin oligomers **2(*n*)**, which can be regarded as structural analogues of fully oxidized PANI (Scheme 2). Analogous structures to **2(*n*)** have only been reported for the dimer as a Ni-complex[41] and, very recently, the trimers as Ni-complexes.[54] We also present the switching of their oxidation states, which is characteristically observed in PANIs.

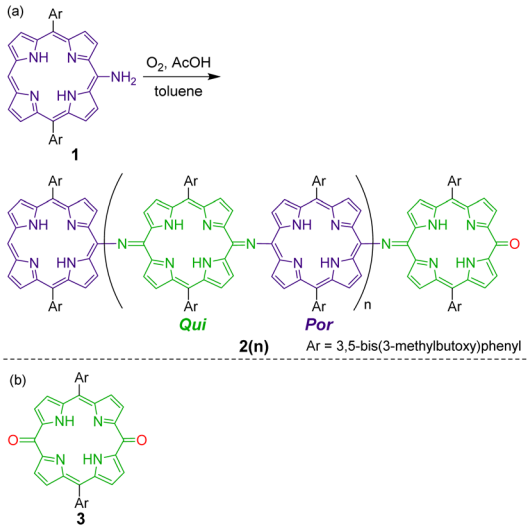

Scheme 2 (a) Oxidative oligomerization of a *meso*-aminoporphyrin **1** that affords fully oxidized polyaniline-type oligomers **2(*n*)**. (b) Chemical structure of a monomeric quinone **3** as a reference compound.

Results and discussion

Oligomerization of *meso*-aminoporphyrin

Meso-aminoporphyrin **1** remains stable in typical organic solvents, such as toluene and chloroform, even at high temperatures.[50] However, we serendipitously discovered that **1** spontaneously oligomerizes in the presence of a weak acid, such as acetic acid (Scheme 2). When a toluene–AcOH solution of **1** was stirred at 100 °C under an oxygen atmosphere, **1** disappeared completely in a few hours because of the formation of the oligomeric products of **1**. MALDI-TOF mass spectrometry of the crude product indicated the formation of a dimeric product of **1** as well as even-numbered oligomeric species (Fig. S3†). We isolated each oligomer using a combination of silica gel column chromatography and a recycling GPC-HPLC system. Based on NMR, mass, and elemental analyses and X-ray diffraction studies, the obtained oligomers were identified to be linear oligomers of **1**, *i.e.*, **2(*n*)**, with a structure analogous to fully oxidized PANIs; that is, half of the porphyrin moieties were oxidized to a quinoid structure, and the porphyrinoid moieties and quinoid moieties were linked alternately *via* imine bonds.

Table 1 summarizes the relationship between the isolated yields of **2(*n*)** and reaction conditions. When the reaction was performed under dilute conditions (solvent, toluene : AcOH at 2 : 1 ratio) at 60 °C, dimer **2(0)** was selectively formed (entry 1). Upon increasing the concentration of **1** (entries 3, 5, and 7) and/or increasing the reaction temperature (entries 2, 4, 6, and 8), the yields of higher oligomers (*e.g.*, **2(1)**, **2(2)**, and **2(3)**) increased, whereas that of **2(0)** decreased. Under a specific condition (entry 8), traces of higher oligomers, up to docosamer **2(9)**, were detected.

Table 1 Relationship between the isolated yield of **2(*n*)** and reaction condition for the oxidative oligomerization of *meso*-aminoporphyrin **1**

					Yield[a] (%)			
Entry	[**1**] (mM)	Solvent	Temp. (°C)	Time (h)	**2(0)**	**2(1)**	**2(2)**	**2(3)**
1	10	Toluene–AcOH (2 : 1)	60	26	82	5	ND	ND
2	10	Toluene–AcOH (2 : 1)	100	4	45	22	1	ND
3	50	Toluene–AcOH (2 : 1)	60	23	64	13	3	ND
4	50	Toluene–AcOH (2 : 1)	100	3	33	23	5	ND
5	100	Toluene–AcOH (2 : 1)	60	15	54	19	4	1
6	100	Toluene–AcOH (2 : 1)	100	3	20	20	9	3
7	200	Toluene–AcOH (2 : 1)	60	15	44	16	7	2
8	200	Toluene–AcOH (2 : 1)	100	3	18	22	10	3[e]
9[b]	10	Toluene–AcOH (2 : 1)	100	4	ND[c]	ND	ND	ND
10	10	Toluene	100	24	ND[c]	ND	ND	ND
11	10	DMF	100	24	ND[c]	ND	ND	ND
12	10	Toluene–TFA (2 : 1)	60	26	ND[c]	ND	ND	ND
13	10	AcOH	100	5	ND[d]	ND	ND	ND

[a] Isolated yields. ND: not detected. [b] Reaction was performed under a N_2 atmosphere. [c] Full recovery of **1**. [d] Undefined products were obtained. [e] Traces of higher oligomers, up to **2(9)**, were detected.

When the reaction was carried out in a nitrogen atmosphere (oxygen-free condition), **2(*n*)** was not formed (entry 9). Moreover, **1** was recovered completely. The results indicate that O_2 is required for the observed oxidative oligomerization reactions. Further, no reaction was observed in the absence of acetic acid (entries 10 and 11), which indicates that an acidic condition is required for the oligomerization of **1**. However, no reaction was observed by the use of trifluoroacetic acid (TFA), *i.e.*, stronger acid (entry 12). Further, the reaction in neat acetic acid afforded undefined oligomeric products (entry 13).

Structural characterization of the oligomers of 1

Although the crystallization of **2(*n*)** for single-crystal X-ray crystallography failed, we could obtain single crystals of the dinickel complex of the dimer, **Ni-2(0)**, and analyse its crystal structure (Fig. 1). In the crystal of **Ni-2(0)**, the $C_{mesoPor}$–N_{imino} bond length is 1.357(9) Å, the $C_{mesoQui}$=N_{imino} bond length is 1.312(9) Å, and the bending angle of the imine moiety ($C_{mesoPor}$–N_{imino}=$C_{mesoQui}$) is 125.4(6)°. The bending angle indicates partial stacking of the two monomer units in the structure. Both moieties were found to have a ruffled conformation, with the degree of ruffling of the porphyrinoid moiety being greater than that of the quinoid one (mean plane deviations defined by 24 core atoms are 0.31 and 0.49 Å for porphyrinoid and quinoid moieties, respectively). The intramolecular Ni···Ni distance was found to be 8.411(4) Å.

Fig. 2 shows the ^{1}H NMR spectra of **2(*n*)** (n = 0, 1, 2, and 3) in $CDCl_3$ recorded at 323 K. The spectrum of **2(0)** has characteristic signals of the aromatic porphyrinoid moiety: four doublet signals for β-protons at approximately 9.12–8.84 ppm, one singlet signal for the *meso*-proton ($H_{por\text{-}meso}$) at 9.86 ppm, and one singlet signal for internal NH protons (NH_{por}) at −2.08 ppm. On the other hand, most of the signals for β-protons of the nonaromatic quinoid moiety ($H_{qui\text{-}meso}$) were considerably broadened. These broad signals sharpened at elevated temperatures and split at low temperatures (Fig. S8†). These changes indicate that the decrease in temperature slows the rotational motion along the N=C_{Qui} double bond and/or the tautomerization of the NH proton in the quinoid unit[49] enough to allow the NMR signal to differentiate. On the other hand, the characteristic signal of the internal NH protons of the quinoid moiety (NH_{qui}) was clearly observed at 13.4 ppm. The integral ratio of each proton signal (especially $H_{por\text{-}meso}$, $H_{por\text{-}\beta}$, NH_{por}, and NH_{qui}) was consistent with the porphyrinoid : quinoid ratio in the molecule.

Similar to the case of **2(0)**, the ratio of the number of porphyrinoid moieties to quinoid moieties in **2(*n*)** (n = 1, 2, and 3) was also determined to be 1 : 1 through ^{1}H NMR analyses. It should be noted that internal NH signals for the end monoiminoporphyrin moiety and the inner diiminoporphyrin moieties could also be unambiguously distinguished (end: *ca.* −2.0 ppm, inner: *ca.* −1.1 ppm).

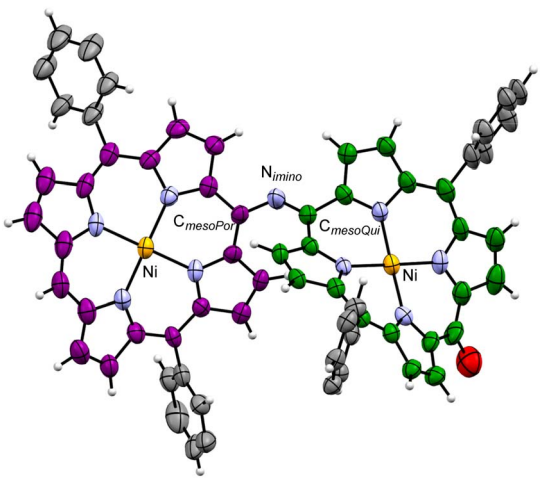

Fig. 1 Thermal ellipsoid representation (40% probability level) of the crystal structure of **Ni-2(0)** (C_{Por} = purple, C_{Qui} = green, C_{Ar} = grey, H = white, N = blue, O = red, and Ni = orange). Substituents on the aryl groups and solvent molecules are omitted for clarity.

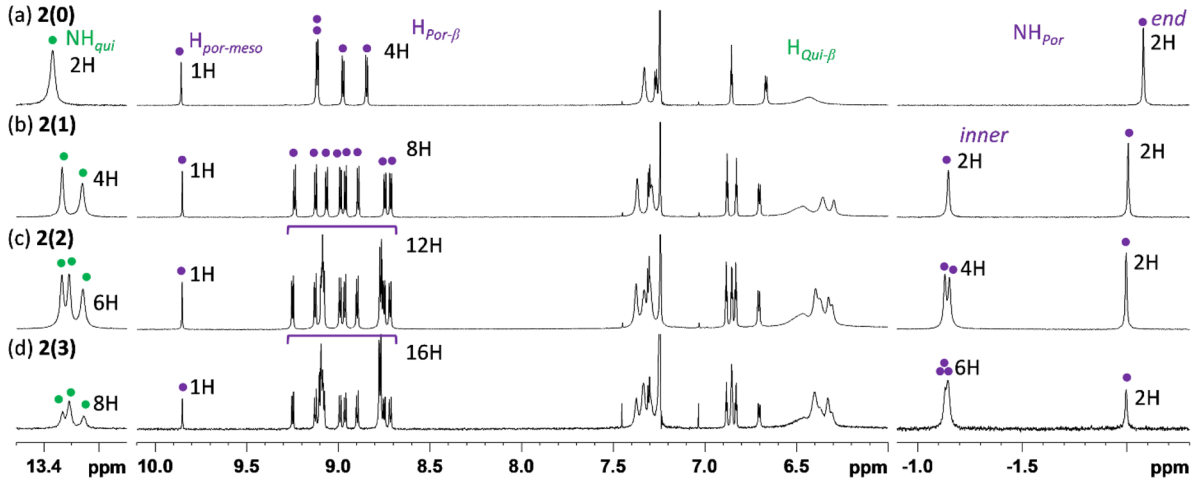

Fig. 2 ^{1}H NMR (500 MHz, $CDCl_3$, 323 K) spectra of (a) **2(0)**, (b) **2(1)**, (c) **2(2)**, and (d) **2(3)**.

Fig. S9† presents the ^{1}H NMR spectrum of **Ni-2(0)** in $CDCl_3$ recorded at various temperatures. A notable feature of **Ni-2(0)** is that the eight quinoid β-protons were observed to be inequivalent in the NMR spectra recorded below room temperature. This result indicates that rotational motion along the N=C$_{Qui}$ double bond is mostly regulated below room temperature and it enabled us to assign most of the signals using 2D NMR techniques (^{1}H COSY and ^{1}H ROESY, Fig. S10 and S11†). The results revealed that two signals for quinoid β-protons appear more upfield (5.5 and 3.6 ppm) than those of others (7.7–6.4 ppm). Considering the molecular structure of **Ni-2(0)**, these two protons are located above the porphyrinoid moieties owing to the bending of the imine bond and are therefore strongly affected by the shielding effect of the diatropic ring current of the aromatic porphyrinoid moieties.

Optical properties

The electronic absorption spectra of **2(*n*)** (Fig. 3, top panel) consisted of a sharp and intense peak at ~427 nm, assignable to the Soret band of the porphyrin unit, and a characteristic broad band between 750 and 1200 nm. As this broad NIR band is absent in the spectra of the monomer components, *i.e.*, **1** and **3**, it was assigned to ICT from electron-rich porphyrinoid moieties to electron-deficient quinoid ones. The peak maximum of the ICT band was almost the same for **2(1)**, **2(2)**, and **2(3)** and was red-shifted relative to that of **2(0)**, indicating a narrower HOMO–LUMO gap of **2(1)**, **2(2)**, and **2(3)** compared to that of **2(0)**. This can be attributed to the contribution of inner diiminoporphyrin moieties with higher HOMO energies than those of the end monoiminoporphyrin moieties. This inference is further supported by electrochemical measurements and theoretical calculations (*vide infra*).

Electrochemical properties

To evaluate the oxidation/reduction potentials and HOMO–LUMO gaps of the oligomers, the electrochemical properties of **2(0)**, **Ni-2(0)**, and **2(1)** were investigated by conducting cyclic voltammetry in CH_2Cl_2 containing 0.1 M ^{n}Bu$_4$NPF$_6$ (Table 2 and Fig. S12†). **2(0)** exhibited the first reversible oxidation wave at 0.42 V and the first reversible reduction waves at −0.98 V, respectively. The first reduction peak was slightly split in two when measured in a different solvent (−0.87 and −0.99 V in ^{n}PrCN). This suggests that the first reduction event is a two-electron process. Considering the redox potential of monomers **1** and **3**, it can be inferred that the oxidation of **2(0)** occurred at the porphyrinoid moiety, whereas reduction occurred at the quinoid moiety. Further, the first oxidation wave of **2(1)** was observed at 0.12 V, which is lower by 0.30 V compared to that of **2(0)**. This suggests a higher HOMO level of **2(1)** derived from the inner diiminoporphyrin moiety. The first reduction wave of **2(1)** was observed at −0.91 V, which is higher

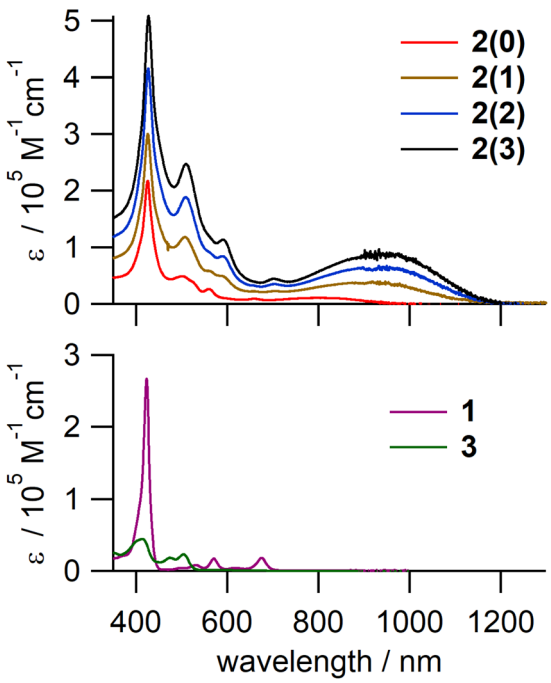

Fig. 3 UV-vis-NIR absorption spectra of **2(*n*)** and the corresponding monomers, **1** and **3**, in toluene.

Table 2 Half-wave potentials (V *vs.* Fc/Fc^+) of **2(0)**, **Ni-2(0)**, **2(1)**, **1**, and **3**. Potentials were determined by cyclic voltammetry

	Solv.	E_{Red2}	E_{Red1}	E_{Ox1}	$E_{Ox1} - E_{Red2}$
2(0)	CH_2Cl_2		−0.98 (2e)	0.42	1.34
Ni-2(0)	CH_2Cl_2	−1.00	−0.82	(0.50)[a]	1.32
2(1)	CH_2Cl_2	−1.33	−0.91	0.12	1.03
1	^{n}PrCN		−1.73	(0.08)[a]	1.81
3	^{n}PrCN	−1.28	−0.78	(1.21)[a]	1.99

[a] Irreversible peak.

by 0.07 V compared to that of **2(0)**. For **Ni-2(0)**, two reversible reduction waves were observed at −0.82 and −1.00 V, and the first reduction potential is higher by 0.16 V compared to that of **2(0)**. This trend is also seen in the first reduction potentials of related monomer quinone reported previously.[52] The first oxidation of **Ni-2(0)** was irreversibly observed.

The HOMO–LUMO gaps estimated by the difference between E_{Ox1} and E_{Red1} are 1.34 eV (1.08×10^4 cm^{-1}, 925 nm) and 1.03 eV (8.30×10^3 cm^{-1}, 1204 nm) for **2(0)** and **2(1)**, respectively. These are narrower than those of monomers **1** and **3** and consistent with the peak maximum of the ICT band in the UV-vis-NIR spectra.

Theoretical calculations

To gain further insights into the electronic states of **2(*n*)**, density functional theory (DFT) calculations were performed on **2′(0)** and **2′(1)** (simplified derivatives in which alkoxy substituents on the phenyl rings were replaced by hydrogen atoms). Selected MOs and the molecular orbital (MO) energy diagrams of **2′(0)** and **2′(1)** are shown in Fig. 4 and Fig. S18,† respectively. As predicted from the electronic properties of each moiety, the HOMO and LUMO of **2′(0)** were dominated by its porphyrinoid and quinoid moieties, respectively. The HOMO of **2′(1)** was dominated by the inner porphyrinoid moiety of the molecular chain, whereas HOMO−1 was dominated by the end porphyrinoid moiety. The energy level of HOMO−1 of **2′(1)** is 0.1 eV higher than that of the HOMO of **2′(1)** while being almost the same as that of the HOMO of **2′(0)**. Both the LUMO and LUMO+1 of **2′(1)** are localized on the quinoid moieties, but the difference between the two quinoid moieties is not as pronounced as in the case of the porphyrinoid moieties.

Time-dependent (TD) DFT calculations were also performed to assign the UV-vis-NIR absorption bands (Tables S3 and S4, and Fig. S19 and S20†). The results suggest that the broad absorption band of **2(*n*)** corresponds to the $S_0 \rightarrow S_1$ transition due to the HOMO–LUMO transition, *i.e.*, the ICT transition. The transition energies of **2′(0)** and **2′(1)** are 826 and 1070 nm, respectively. This difference is due to the higher energy level of the HOMO of **2′(1)**, and is consistent with the experimental absorption.

Plausible reaction mechanism for the oxidative oligomerization of 1

The reaction mechanism of the oligomerization of **1** might essentially be the same as that of the oxidative oligomerization of aniline to PANIs, and it might involve nucleophilic substitution reactions involving porphyrin π–cation radicals[55,56] (Scheme 3). Because of its low oxidation potential, **1** would undergo single-electron oxidation by dioxygen to form the corresponding cation radical $\mathbf{1}^{\bullet+}$. According to the DFT calculations of $\mathbf{1}'^{\bullet+}$ (Fig. S21†), the carbon atoms at the *meso*-positions have a high spin density. Therefore, the subsequent nucleophilic attack of the amino group of **1** occurs at the free *meso*-position of $\mathbf{1}^{\bullet+}$ to generate the all-porphyrinoid dimeric products. This intermediate dimer should readily undergo single-electron oxidation to form a cation radical, which either undergoes further nucleophilic attack by **1** to form a trimeric product or single-electron oxidation to form **2(0)** after the replacement of the unstable terminal imine (C=NH) with the carbonyl (C=O) group.

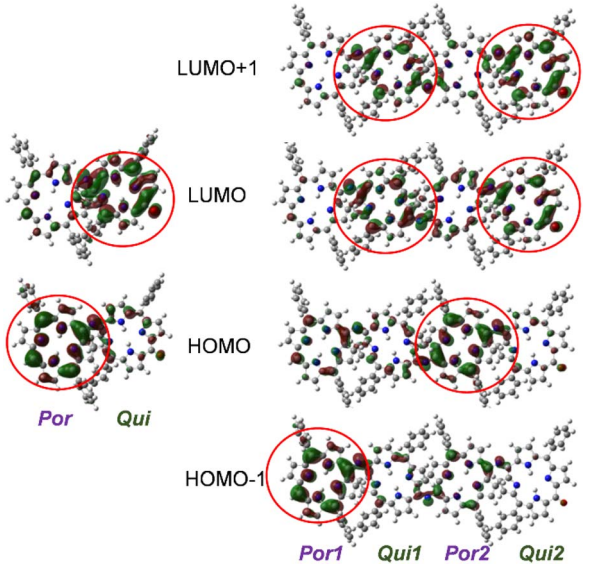

Fig. 4 Frontier orbitals **2′(0)** and **2′(1)** (B3LYP-D3/6-31G(d,p)).

Considering the higher first oxidation potential of **2(*n*)** relative to that of **1**, the porphyrinoid moieties next to the quinoid moieties are considered to be less susceptible to oxidation under the reaction conditions. Therefore, no further elongation of **2(*n*)** is possible. On the other hand, an odd-numbered oligomer contains at least one porphyrinoid moiety without quinoid moieties on both sides and is therefore prone to oxidize under the reaction conditions. Therefore, further elongation of an odd-numbered oligomer is possible. Scheme 3 shows an example of the elongation of the trimer to tetramer.

Experimental results (Table 1) show that the oligomerization reaction proceeds in the presence of weak acids such as acetic acid (and from preliminary experiments, formic acid), but the role of weak acids is not yet clear. In the case of using trifluoroacetic acid (TFA), the reaction does not proceed at all and **1** is completely recovered. In the presence of TFA, the colour of **1** turns green, indicating the protonation of the inner nitrogen atoms of porphyrin macrocycles. *N*-Protonation of porphyrins results in a significant increase in their oxidation potential.[57,58] This is consistent with the experimental results that **1** does not

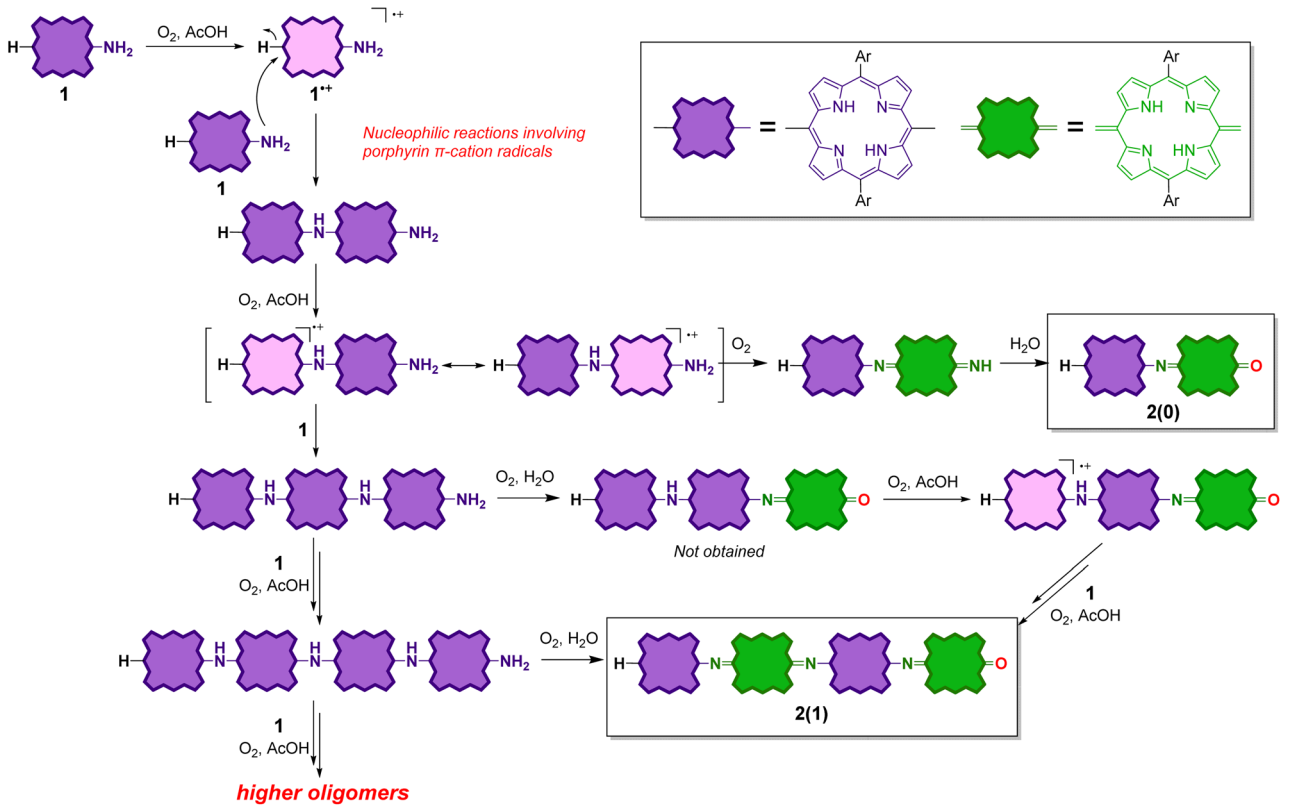

Scheme 3 Plausible reaction mechanism for the oligomerization of **1**.

undergo oxidative oligomerization reactions in the presence of TFA. On the other hand, no significant change in the colour of **1** is observed in acetic acid, suggesting that the inner nitrogen atoms of **1** are not protonated. Therefore, the hydrogen bonding of an acetic acid molecule to the amino group on **1** may induce the oxidation of **1** by oxygen.

Reduction of the fully oxidized dimer

Because quinoid moieties can be readily reduced by mild reducing agents,[47,52] the chemical reduction of **2(0)** and **2(1)** was examined to obtain reduced PANI-type derivatives (Schemes 4 and 5). When **2(0)** was treated with sodium ascorbate in a polar solvent (*e.g.*, $CDCl_3$/DMSO-d_6), the initial brown solution turned green. In the electronic absorption spectrum of the resulting solution, the broad ICT band was not observed; instead, two new peaks appeared at 650–700 nm. The ^{1}H NMR spectrum of the reduced product (Fig. S13†) exhibited eight doublet peaks in the 9.0–7.6 ppm range and two singlet peaks at −0.6 and −1.6 ppm; the characteristic peaks of the quinoid moiety had disappeared (*e.g.*, the broad singlet at 13.3 ppm). The NMR results indicate that the quinoid moiety in **2(0)** was reduced to porphyrinoid, resulting in all-porphyrinoid dimer **4a**. The characteristic singlet signal at 11.4 ppm was assigned to the bridge NH proton.[44,45]

Further, the colour of the reduced sample turned brown upon standing in an aerobic atmosphere within several hours. The ^{1}H NMR spectrum of the resultant solution indicated that the reduced dimer **4a** had reverted to the original oxidized form, **2(0)** by aerobic oxidation. The switching of the oxidation state of the dimer could be repeated at least twice (Fig. S13†).

The air-sensitive reduced dimer **4a** was stabilized by the *in situ* alkylation of its terminal hydroxyl group.[49] The *in situ*

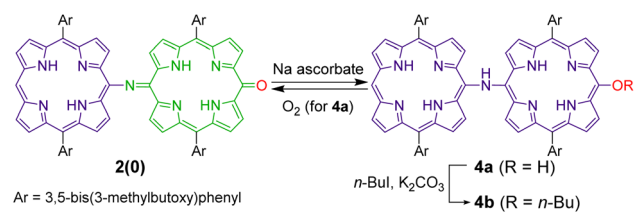

Scheme 4 Redox switching between **2(0)** and **4a**, and etherification of the hydroxyl group of **4a**.

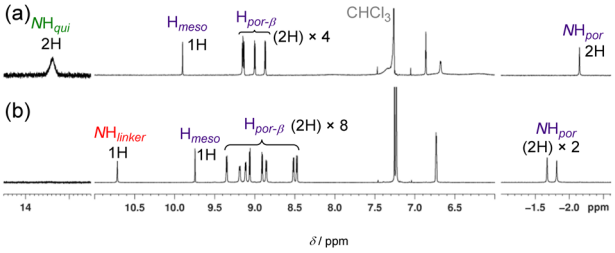

Fig. 5 ^{1}H NMR (500 MHz, $CDCl_3$) spectra of (a) **2(0)** and (b) **4b**.

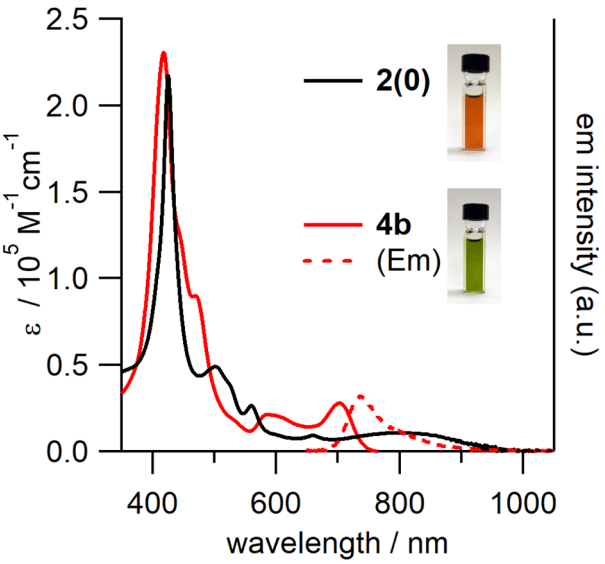

Fig. 6 UV-vis-NIR absorption spectra of **2(0)** and **4b** and the fluorescence spectrum of **4b** (excited at 430 nm) in toluene.

alkylation of **4a** using 1-iodobutane resulted in butoxy-substituted dimer **4b** in 79% yield (from **2(0)**). **4b** was sufficiently stable against aerobic oxidation to be purified by silica gel column chromatography.

The structure of **4b** was determined using ^{1}H NMR, high-resolution electrospray ionisation mass spectroscopy (ESI-HRMS), and elemental analyses. The ^{1}H NMR spectrum of **4b** (Fig. 5) in $CDCl_3$ revealed the disappearance of the characteristic NH and β signals of the quinoid moiety and the presence of two porphyrinoid moieties. The signal of the bridge NH proton was observed at 10.7 ppm.

In the UV-vis-NIR absorption spectrum of **4b** (Fig. 6), the characteristic ICT band of **2(0)** could no longer be observed; the spectrum contained broad Soret and Q bands. In addition, **4b** exhibited broad fluorescence in the 680–1000 nm range with a peak maximum of 738 nm.

Reduction of the fully oxidized tetramer

The reduction of tetramer **2(1)** was also conducted in the same manner as **2(0)** (Scheme 5). The reduction of **2(1)** with sodium ascorbate resulted in fully reduced tetramer **5a** as the sole product. The ^{1}H NMR spectrum of this product is shown in Fig. S14.† Similar to reduced dimer **4a**, **5a** was unstable against aerobic oxidation; it readily oxidized during the workup process to form partially oxidized tetramer **6** with one quinoid moiety at the chain end. It is noteworthy that **6** was moderately stable in air; the oxidation of the inner porphyrinoid moiety in **6** to generate tetramer **2(1)** in the solution required more than two days. This result indicates that the inner porphyrinoid moieties in **5a** and **6** are less susceptible to air oxidation than the end porphyrinoid moiety. This inference is reasonable because *meso*-bis(*N*-arylamino)porphyrins are isolable,[54,55,59,60] whereas *meso*-diaminoporphyrin readily undergoes aerobic oxidation to the corresponding quinone.[50]

Further, the end hydroxyl group in fully reduced tetramer **5a** was acetylated to stabilize it. The crude acetylated product of **5a** contained the desired product, **5b** along with two partially oxidized products, **7a** and **7b** (1 : 1 mixture) with one inner

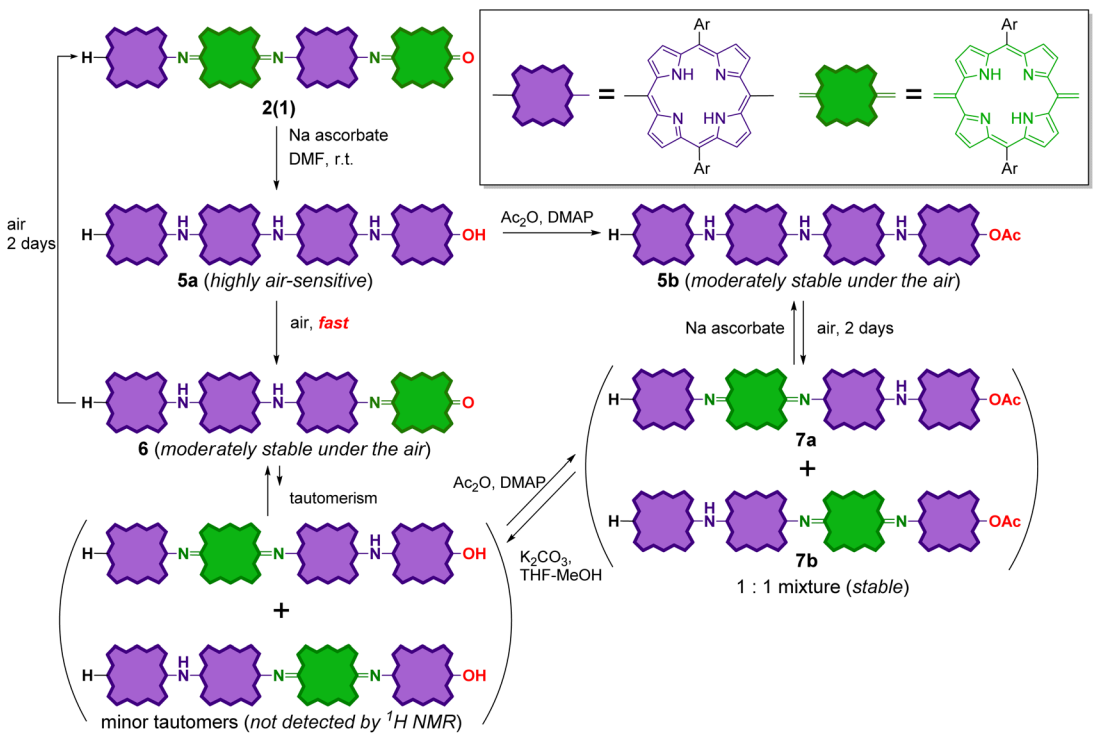

Scheme 5 Redox switching of the tetramer.

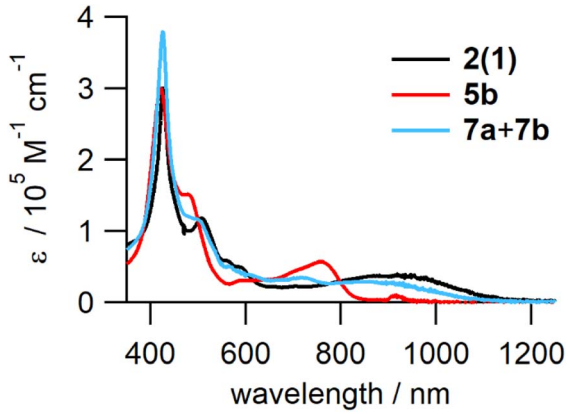

Fig. 7 UV-vis-NIR absorption spectra of **2(1)**, **5b**, and the mixture of **7a** and **7b** in toluene.

quinoid moiety. **5b** and the mixture of **7a** and **7b** could be readily isolated by column chromatography. Similar to partially oxidized tetramer **6**, **5b** was moderately stable in air, and its aerobic oxidation in solution to afford a mixture of **7a** and **7b** required more than two days. **7** could be reduced with sodium ascorbate to obtain **5b** again. That is, the interconversion between **5b** and **7** was reversible.

It should also be noted that **6** and **7** could also be reversibly interconverted. When **6** was treated with acetic anhydride, a mixture of **7a** and **7b** was formed. Under the same reaction conditions, no reaction proceeded in the cases of fully oxidized forms **2(0)** and **2(1)**. The removal of the terminal acetyl group in **7a** and **7b** (1 : 1 mixture) by basic hydrolysis resulted in the formation of **6** as the sole product. Therefore, the interconversion between **6** and **7** can be rationalized by considering the equilibrium between **6** and its tautomers with end hydroxyl groups, whose NMR signals were below the lower limit of detection (Scheme 5).

The structures of the reduced tetramers were confirmed by ^{1}H NMR (Fig. S13†). The UV-vis-NIR absorption spectra of **2(1)**, **5b**, and the mixture of **7a** and **7b** are shown in Fig. 7. Similar to reduced dimer **4**, the fully reduced tetramer, **5b** did not exhibit the characteristic ICT band in the NIR region; the spectrum contained strong Q bands at ~780 nm. However, the partially reduced tetramers (**7a** and **7b**) exhibited an ICT band, but the extinction coefficient of this band was smaller than that of **2(1)** owing to the decrease in the number of quinoid moieties in the partially reduced molecules.

Solvent-dependent dynamic behaviours of the partially reduced tetramers

Considering the reaction mechanism for the formation of **7** from **6**, the position of the quinoid moieties in the partially reduced oligomers is considered to change dynamically in the solution. This quinoid transfer within the molecule involves intramolecular (proton-coupled) electron transfer. It should therefore be related to the electronic conductivity of the partially oxidized PANI analogue. Therefore, the interconversion of the partially reduced tetramers, **7a** and **7b** in solution

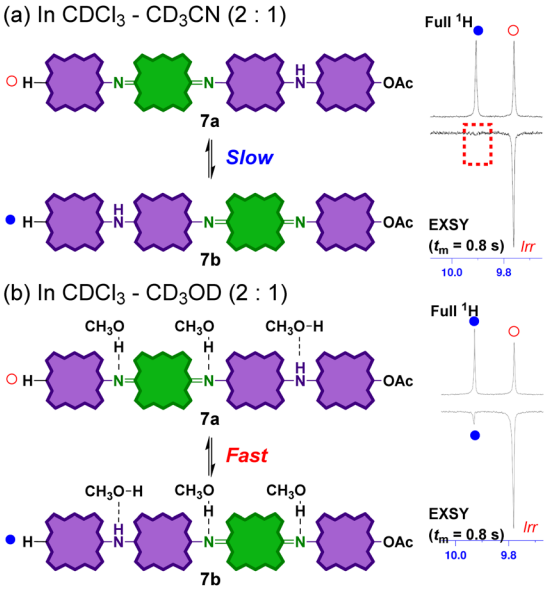

Fig. 8 ^{1}H 1D EXSY NMR spectra (500 MHz, 300 K) of an equilibrium mixture of **7a** and **7b** in (a) $CDCl_3$–CD_3CN (2 : 1) and (b) $CDCl_3$–CD_3OD (2 : 1). Mixing time t_m = 0.8 s.

was evaluated by ^{1}H 1D-exchange spectroscopy (EXSY; Fig. 8). A pair of sharp singlet signals of the *meso*-proton of the end porphyrinoid moieties at ~9.8 ppm was selected for EXSY measurements. In $CDCl_3$ or $CDCl_3$/CD_3CN (2 : 1), no correlation was observed within 0.4–1.0 s of mixing time (t_m) at 300 K (Fig. 8a). This result indicates that the interconversion rates were significantly low in these solvents. In contrast, a clear correlation was observed in $CDCl_3$/CD_3OD (2 : 1) (Fig. 8). The interconversion of **7a** and **7b** not only involved electron transfer but also proton transfer *via* the bridged nitrogen atoms. Considering that the conductivity of partially oxidized PANI was significantly enhanced in acidic media owing to *N*-protonation,[4–10] the enhanced interconversion between **7a** and **7b** can be rationally explained by the hydrogen-bonding of CD_3OD to the bridged nitrogen atoms.

To estimate the activation barrier of this interconversion, the interconversion rate constants were determined by conducting ^{1}H 1D EXSY measurements (see Fig. S15 and S16, and Table S2†) at different temperatures (278, 298, and 318 K). The interconversion rate constant increased at an elevated temperature. The Eyring plot of the rate is shown in Fig. S17,† from which the kinetic parameters were determined as $\Delta H^{\ddagger} = 26.9 \pm 5.5$ kJ mol^{-1} (6.4 ± 1.3 kcal mol^{-1}), $\Delta S^{\ddagger} = -169 \pm 19$ J mol^{-1} K^{-1} (-40.4 ± 4.4 cal mol^{-1} K^{-1}), and $\Delta G^{\ddagger}_{298\ K} = 77.3 \pm 7.8$ kJ mol^{-1} (18.5 ± 1.9 kcal mol^{-1}).

Conclusions

We presented the synthesis and reversible redox switching of novel linear π-conjugated *meso*-aminoporphyrin oligomers, which are analogous to PANIs. The *meso*-aminoporphyrin undergoes oxidative oligomerization in the presence of dioxygen and an acid catalyst to afford oligomers with a structure

similar to that of fully oxidized PANI (pernigraniline). The obtained fully oxidized oligomers have narrow HOMO–LUMO gaps and broad NIR electronic absorption assignable to ICT from porphyrinoid to quinoid moieties (HOMO–LUMO transition). The fully oxidized oligomers could be reversibly reduced with sodium ascorbate to obtain the corresponding reduced oligomers that do not exhibit the ICT absorption but the emission in the NIR region. Finally, we also demonstrated that the internal transfer of the quinoid moiety in the partially reduced tetramer was significantly enhanced in the presence of a protic solvent. We believe that these results are directly related to the high electronic conductivities of partially oxidized PANIs by *N*-protonation.

The *meso*-aminoporphyrin oligomers discussed herein are a novel type of π-conjugated porphyrin oligomers/polymers, whose properties can be switched by redox stimulation. In the future, we plan to obtain *meso*-aminoporphyrin polymer films to explore their properties, such as their conductivity with a view to developing applications for sensors using their NIR absorption/luminescence properties, functional electrodes and electrochemical catalysts. A study on modulating the properties of *meso*-aminoporphyrin oligomers by metal insertion is also in progress.

Data availability

All necessary data have been included in the manuscript and in the ESI.†

Author contributions

K. Y. and K. S. supervised and administrated this project. S. T. discovered the reactions and prepared the compounds. S. T. also conducted the basic NMR, MS, spectroscopic, and electrochemical analyses. K. Y. conducted X-ray diffraction analyses, EXSY NMR analyses, and DFT calculations. K. Y. and S. T. wrote the manuscript, and K. S. reviewed and edited it.

Conflicts of interest

There are no conflicts to declare.

Acknowledgements

We thank Prof. Dr Motoko S. Asano (Gunma University) for the helpful discussion. The computation was performed using Research Center for Computational Science, Okazaki, Japan (Projects: 20-IMS-C195, and 21-IMS-C218).

Notes and references

1 D. Kumar and R. C. Sharma, *Eur. Polym. J.*, 1998, **34**, 1053–1060.
2 A. B. Kaiser, *Rep. Prog. Phys.*, 2001, **64**, 1–49.
3 S. Tajik, H. Beitollahi, F. G. Nejad, I. S. Shoaie, M. A. Khalilzadeh, M. S. Asl, Q. Van Le, K. Zhang, H. W. Jang and M. Shokouhimehr, *RSC Adv.*, 2020, **10**, 37834–37856.
4 A. G. MacDiarmid and A. J. Epstein, *Faraday Discuss. Chem. Soc.*, 1989, **88**, 317–332.
5 A. J. Epstein and A. G. MacDiarmid, *Synth. Met.*, 1995, **69**, 179–182.
6 *Fundamentals and Emerging Applications of Polyaniline*, ed. M. Mozafari and N. P. S. Chauhan, Elsevier, 2019.
7 E. M. Geniès, A. Boyle, M. Lapkowski and C. Tsintavis, *Synth. Met.*, 1990, **36**, 139–182.
8 J. Stejskal and R. G. Gilbert, *Pure Appl. Chem.*, 2002, **74**, 857–867.
9 N. Gospodinova and L. Terlemezyan, *Prog. Polym. Sci.*, 1998, **23**, 1443–1484.
10 Z. Wei and C. F. J. Faul, *Macromol. Rapid Commun.*, 2008, **29**, 280–292.
11 K. M. Molapo, P. M. Ndangili, R. F. Ajayi, G. Mbambisa, S. M. Mailu, N. Njomo, M. Masikini, P. Baker and E. I. Iwuoha, *Int. J. Electrochem. Sci.*, 2012, **7**, 11859–11875.
12 Z. A. Boeva and V. G. Sergeyev, *Polym. Sci., Ser. C*, 2014, **56**, 144–153.
13 S. K. Dhawan, D. Kumar, M. K. Ram, S. Chandra and D. C. Trivedi, *Sens. Actuators, B*, 1997, **40**, 99–103.
14 G. Wu, K. L. More, C. M. Johnston and P. Zelenay, *Science*, 2011, **332**, 443–447.
15 M. B. Regasa, T. R. Soreta, O. E. Femi, P. C. Ramamurthy and S. Kumar, *J. Mol. Recognit.*, 2020, **33**, 1–11.
16 Z. Li and L. Gong, *Materials*, 2020, **13**, 548.
17 R. Willstätter and C. W. Moore, *Ber. Dtsch. Chem. Ges.*, 1907, **40**, 2665–2689.
18 R. A. Singer, J. P. Sadighi and S. L. Buchwald, *J. Am. Chem. Soc.*, 1998, **120**, 213–214.
19 Y. Yu, H. Mao, L. Chen, X. Lu, W. Zhang and Y. Wei, *Macromol. Rapid Commun.*, 2004, **25**, 664–668.
20 I. Różalska, P. Kułyk and I. Kulszewicz-Bajer, *New J. Chem.*, 2004, **28**, 1235–1243.
21 R. Eelkema and H. L. Anderson, *Macromolecules*, 2008, **41**, 9930–9933.
22 D. Qiu, Y. Cheng and L. Wang, *Dalton Trans.*, 2009, 3247.
23 A. H. Arévalo, H. Fernández, J. J. Silber and L. Sereno, *Electrochim. Acta*, 1990, **35**, 741–748.
24 D. K. Moon, K. Osakada, T. Maruyama, K. Kubota and T. Yamamoto, *Macromolecules*, 1993, **26**, 6992–6997.
25 B. C. Roy, M. Dutta Gupta, L. Bhowmik and J. K. Ray, *Bull. Mater. Sci.*, 2003, **26**, 633–637.
26 M. Horie, I. Yamaguchi and T. Yamamoto, *Macromolecules*, 2006, **39**, 7493–7501.
27 W. A. Badawy, K. M. Ismail and S. S. Medany, *Electrochim. Acta*, 2006, **51**, 6353–6360.
28 N. Oyama, K. Hirabayashi and T. Ohsaka, *Bull. Chem. Soc. Jpn.*, 1986, **59**, 2071–2080.
29 T. Ohsaka, K. Hirabayashi and N. Oyama, *Bull. Chem. Soc. Jpn.*, 1986, **59**, 3423–3429.
30 H. L. Anderson, *Chem. Commun.*, 1999, 2323–2330.
31 T. Tanaka and A. Osuka, *Chem. Soc. Rev.*, 2015, **44**, 943–969.
32 H. L. Anderson, S. J. Martin and D. D. C. Bradley, *Angew. Chem., Int. Ed. Engl.*, 1994, **33**, 655–657.

33 P. N. Taylor, J. Huuskonen, R. T. Aplin, H. L. Anderson, J. Huuskonen, G. Rumbles and E. Williams, *Chem. Commun.*, 1998, 909–910.
34 A. Tsuda and A. Osuka, *Science*, 2001, **293**, 79–82.
35 A. Tsuda, H. Furuta and A. Osuka, *Angew. Chem., Int. Ed.*, 2000, **39**, 2549–2552.
36 A. Bettelheim, B. A. White, S. A. Raybuck and R. W. Murray, *Inorg. Chem.*, 1987, **26**, 1009–1017.
37 K. A. Macor, Y. O. Su, L. A. Miller and T. G. Spiro, *Inorg. Chem.*, 1987, **26**, 2594–2598.
38 S. Lamare, S. M. Aly, D. Fortin and P. D. Harvey, *Chem. Commun.*, 2011, **47**, 10942.
39 P. A. Liddell, M. Gervaldo, J. W. Bridgewater, A. E. Keirstead, S. Lin, T. A. Moore, A. L. Moore and D. Gust, *Chem. Mater.*, 2008, **20**, 135–142.
40 M. Gervaldo, P. A. Liddell, G. Kodis, B. J. Brennan, C. R. Johnson, J. W. Bridgewater, A. L. Moore, T. A. Moore and D. Gust, *Photochem. Photobiol. Sci.*, 2010, **9**, 890.
41 L. J. Esdaile, P. Jensen, J. C. McMurtrie and D. P. Arnold, *Angew. Chem., Int. Ed.*, 2007, **46**, 2090–2093.
42 B. Bašić, J. C. McMurtrie and D. P. Arnold, *Eur. J. Org. Chem.*, 2010, 4381–4392.
43 B. Bašić, J. C. McMurtrie and D. P. Arnold, *J. Porphyrins Phthalocyanines*, 2010, **14**, 481–493.
44 L. J. Esdaile, M. O. Senge and D. P. Arnold, *Chem. Commun.*, 2006, **2**, 4192–4194.
45 A. M. V. M. Pereira, M. G. P. M. S. Neves, J. A. S. Cavaleiro, C. Jeandon, J. Gisselbrecht, S. Choua and R. Ruppert, *Org. Lett.*, 2011, **13**, 4742–4745.
46 K. Merahi, A. M. V. M. Pereira, C. Jeandon, L. Ruhlmann, J. A. S. Cavaleiro, M. G. P. M. S. Neves, M. Orio, P. Turek, S. Choua and R. Ruppert, *J. Porphyrins Phthalocyanines*, 2016, **20**, 1233–1243.
47 D. Shimizu, Y. Ide, T. Ikeue and A. Osuka, *Angew. Chem., Int. Ed.*, 2019, **58**, 5023–5027.
48 K. Yamashita, K. Kataoka, M. S. Asano and K. Sugiura, *Org. Lett.*, 2012, **14**, 190–193.
49 K. Yamashita, D. Hirano, M. S. Asano and K. Sugiura, *Chem. Lett.*, 2014, **43**, 1049–1051.
50 K. Yamashita, K. Kataoka, S. Takeuchi and K. Sugiura, *J. Org. Chem.*, 2016, **81**, 11176–11184.
51 K. Yamashita, S. Sakamoto, A. Suzuki and K. Sugiura, *Chem.–Asian J.*, 2016, **11**, 1004–1007.
52 K. Yamashita, D. Hirano and K. Sugiura, *Eur. J. Inorg. Chem.*, 2020, 3507–3516.
53 K. Yamashita, D. Hirano, K. Fujimaki and K. Sugiura, *Chem.–Asian J.*, 2020, **15**, 3037–3043.
54 K. Wang, B. Xiao, L. Xu, M. Zhou, T. Tanaka, A. Osuka and J. Song, *Chin. Chem. Lett.*, 2022, **33**, 4545–4548.
55 D.-M. Shen, C. Liu, X.-G. Chen and Q.-Y. Chen, *J. Org. Chem.*, 2009, **74**, 206–211.
56 C. H. Devillers, A. K. D. Dime, H. Cattey and D. Lucas, *Chem. Commun.*, 2011, **47**, 1893–1895.
57 J. H. Fuhrhop, K. M. Kadish and D. G. Davis, *J. Am. Chem. Soc.*, 1973, **95**, 5140–5147.
58 G. B. Maiya and V. Krishnan, *Inorg. Chem.*, 1985, **24**, 3253–3257.
59 Y. Chen and X. P. Zhang, *J. Org. Chem.*, 2003, **68**, 4432–4438.
60 K. Ladomenou, T. Lazarides, M. K. Panda, G. Charalambidis, D. Daphnomili and A. G. Coutsolelos, *Inorg. Chem.*, 2012, **51**, 10548–10556.